THE JOURNAL OF PHYSICAL CHEMISTRY LETTERS
A JOURNAL OF THE AMERICAN CHEMICAL SOCIETY

pubs.acs.org/JPCL Letter

Molecular-Orbital Framework of Two-Electron Processes: Application to Auger and Intermolecular Coulomb Decay

Nayanthara K. Jayadev, Wojciech Skomorowski, and Anna I. Krylov*

Cite This: J. Phys. Chem. Lett. 2023, 14, 8612−8619 Read Online

ACCESS | Metrics & More | Article Recommendations | Supporting Information

ABSTRACT: States with core- or inner-shell vacancies, which are commonly created by absorption of high-energy photons, can decay by a two-electron process in which one electron fills the core hole and the second one is ejected. These processes accompany many X-ray spectroscopies. Depending on the nature of the initial core- or inner-shell-hole state and the decay valence-hole state, these processes are called Auger decay, intermolecular Coulomb decay, or electron-transfer-mediated decay. To connect many-body wave functions of the initial and final states with the molecular orbital picture of the decay, we introduce the concept of natural Auger orbitals (NAOs). NAOs are obtained by a two-step singular value decomposition of the two-body Dyson orbitals, reduced quantities that enter the expression of the decay rate in the Feshbach−Fano treatment. NAOs afford chemical insight and interpretation of the high-level ab initio calculations of Auger decay and related two-electron relaxation processes.

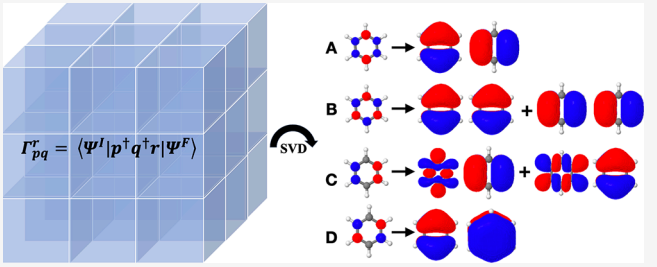

Downloaded via Anna Krylov on September 20, 2023 at 14:11:07 (UTC).
See https://pubs.acs.org/sharingguidelines for options on how to legitimately share published articles.

Molecular-orbital framework is of central importance in chemistry as well as in atomic, molecular, and optical physics.[1] Molecular orbitals explain bonding in molecules and the mechanisms of chemical reactions. Molecular orbitals are also essential for understanding light−matter interactions—they enable predictions of trends in spectroscopic cross sections (e.g., absorption, fluorescence, and phosphorescence), angular-resolved quantities (polarization of the transitions, photoelectron angular distributions), and virbational line-shapes of various electronic transitions (e.g., Franck−Condon factors). Molecular orbitals determine experimental observables and, conversely, their shapes can be extracted from properly designed experimental measurements.[2−4] Hence, molecular orbitals are not just a mathematical construct—they represent physical reality that can be probed experimentally.[1]

Theoretically, molecular orbitals can be derived from general many-body wave functions,[1] and—contrary to the common misconception—are not restricted to low-level treatments, such as Hartree−Fock or Kohn−Sham density functional theories. The definition of appropriate orbitals depends on the type of a physical process rather than the electronic states themselves.[1] That is, different observables give rise to different definitions of orbitals. For example, photoionization or photodetachment processes are described by Dyson orbitals,[5−10] one-photon photoexcitation or emission is described by natural transition orbital (NTOs),[11,12] and spin-forbidden processes such as phosphorescence, intersystem crossing, or magnetic anisotropy give rise to spin−orbit NTOs.[13] Nonlinear processes, such as two-photon (2PA) absorption, hyperpolarizabilities, and resonance inelastic X-ray scattering (RIXS), are described by the perturbed NTOs.[14−17] A brief history of NTOs and related analyses is given in ref 1 (in particular, footnote 57).

The definition of such physically relevant orbitals for many-body wave functions is based on reduced quantities, such as reduced density matrices,[18−20] that enter the expressions for the observables. Figure 1a illustrates this idea for the photoionization/photodetachment process. The key element entering the cross-section expression[8,21] (called photoelectron matrix element) can be written as a matrix element of the dipole operator between the Dyson orbital and the wave function of the ejected electron. Dyson orbitals can be described as a generalized overlap between the initial (N-electron) and final ($N-1$ electron) states:

$$\phi^d(x_1) = \sqrt{N} \int \Psi^I(x_1, x_2, ..., x_N)\Psi^F(x_2, ..., x_N)\mathrm{d}x_2 ... \mathrm{d}x_N \quad (1)$$

Using Dyson amplitudes (shown in Figure 1a), Dyson orbital can be expressed in terms of canonical Hartree−Fock molecular orbitals

$$\phi^d(x) = \sum_p \gamma_p \phi_p(x) \quad (2)$$

Received: July 16, 2023
Accepted: August 30, 2023

© XXXX American Chemical Society

https://doi.org/10.1021/acs.jpclett.3c01966
J. Phys. Chem. Lett. 2023, 14, 8612−8619

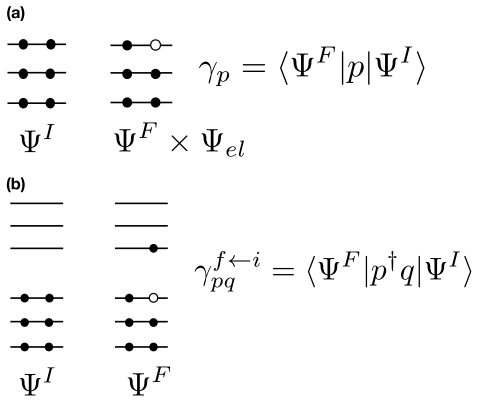

Figure 1. Essential information on a transition between the many-body initial and final states is contained in reduced quantities. Panel (a): Initial and final states in photoionization/photodetachment processes. These states are connected by a one-electron Dyson orbital (the definition of the Dyson orbital amplitudes is given on the right). Panel (b): Initial and final states in one-photon absorption processes. These states are connected by a one-particle transition density matrix (equation on the right).

or any other set of orbitals used to represent the many-body wave functions. The norms of Dyson orbitals, which quantify the one-electron character of the transitions, can be used in lieu of photoelectron intensities (pole strengths).

This simplification of the original expression—dipole matrix element between the two many-body wave functions—is possible because electrons are indistinguishable and the integration can be carried out in two steps. Dyson orbitals describe the difference between the N and $N-1$ electron wave functions and can be computed for wave functions described by any level of theory, including the exact ones. Hence, they represent the generalization of canonical Hartree–Fock orbitals to a many-body framework.[1,10]

Figure 1b shows a one-particle transition density matrix connecting the ground and excited states. This object contains all the information needed to compute the transition dipole moment for one-photon electronic transitions, such as those involved in UV–vis or X-ray absorption or emission processes. The density matrix can be collapsed to the most compact form using singular value decomposition (SVD), a procedure analogous to matrix diagonalization

$$\gamma^{f \leftarrow i} = U \Sigma V^T \tag{3}$$

where Σ is a diagonal matrix containing singular values and matrices U and V are unitary matrices, so that the transition density—often referred to as an exciton wave function[22−24]—can be represented as sum of pairs of hole and particle orbitals:

$$\rho^{tr}(x_\mathrm{p}, x_\mathrm{h}) = \sum_{rs} \gamma_{rs}^{f \leftarrow i} \phi_r(x_\mathrm{p}) \phi_s(x_\mathrm{h}) = \sum_K \sigma_K \psi_K^\mathrm{p}(x_\mathrm{p}) \psi_K^\mathrm{h}(x_\mathrm{h}) \tag{4}$$

where σ_K are singular values (elements of the diagonal matrix Σ) and $\psi_K^\mathrm{h}(x_\mathrm{h})/\psi_K^\mathrm{p}(x_\mathrm{p})$ are the corresponding hole and particle NTOs:

$$\psi_K^\mathrm{h}(x) = \sum_q V_{qK} \phi_q(x) \tag{5}$$

$$\psi_K^\mathrm{p}(x) = \sum_q U_{qK} \phi_q(x) \tag{6}$$

The norm of γ, which can be evaluated as

$$\|\gamma^{f \leftarrow i}\| = \sqrt{\sum_K \sigma_K^2} \tag{7}$$

quantifies the one-electron character of the transition, similarly to the norms of Dyson orbitals. In molecules, typically only a small number of singular values are nonzero, whereas collective excitations (plasmons) are characterized by many contributions with similar weights.[25] By using NTOs, the intrinsic character of electronic transitions can be revealed and visualized.

The concept of NTOs was extended to spin-forbidden transitions by using spinless density matrices that enter the expressions of spin–orbit coupling between two multiplets,[13] to nonlinear properties, such as 2PA or RIXS, by using perturbed transition density matrices,[14,15] metastable electronic states,[9,26] and so on.[16,17]

Here we introduce natural orbitals for two-electron processes, such as Auger–Meitner decay[27,28] and related phenomena—Interatomic Coulomb decay (ICD)[29,30] and electron-transfer-mediated decay (ETMD).[31] Auger decay accompanies many X-ray induced processes and entails filling a core vacancy by a valence electron with a simultaneous ejection of the second valence electron (Figure 2). This is the

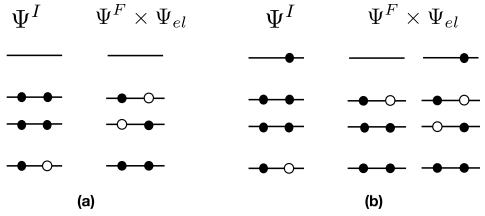

Figure 2. Initial and final states in regular (a) and resonant (b) Auger decay. The two decay configurations in panel (b) correspond to the participator and spectator decay, respectively.

main relaxation channel of core-excited or core-ionized states in molecules composed of light atoms. It is exploited in many spectroscopies and in applications (e.g., in radiotherapy and precision medicine[32−35]). ICD and ETMD operate in a similar way, the main difference being that the initial hole and the two electrons involved in the relaxation process belong to the two nearby molecules; for example, the two valence hole states in the final ICD state are located on two different molecules. Importantly, ICD can occur when local decay is not energetically possible, such as often happens for inner-shell vacancies.[30]

Although primary Auger processes—such as shown in Figure 2—result in the ejection of one electron, they cannot be described by the Dyson orbitals suitable for photoionization/photodetachment, eq 1. This is because Auger decay is an inherently two-electron process—to connect the initial core-hole state and the final state, two electrons need to change their states (Figure 2). Mathematically, it means that this transition requires three creation/annihilation operators, giving rise to two-body Dyson orbitals (or Dyson geminals):[36−39]

$$\Gamma_{qr}^{p} = \langle \Psi^F | p^\dagger q r | \Psi^I \rangle \tag{8}$$

$$\Gamma_{r}^{pq} = \langle \Psi^I | p^\dagger q^\dagger r | \Psi^F \rangle \tag{9}$$

https://doi.org/10.1021/acs.jpclett.3c01966
J. Phys. Chem. Lett. 2023, 14, 8612−8619

where Ψ^I is the initial core-hole state and Ψ^F is the final state. In Hermitian theories, Γ^p_{qr} and Γ^{pq}_r are conjugates of each other, but in EOM-CC the two objects are distinct and both need to be computed for evaluation of decay rates.[36] For nonresonant Auger decay (Figure 2a) Ψ^I is a core-ionized state and Ψ^F is a valence doubly ionized state. For resonant Auger decay (Figure 2b) Ψ^I is the core-excited state and Ψ^F is the valence ionized state. To describe core-vacancy states, we use EOM-CCSD combined with with core−valence separation (CVS) scheme:[40] CVS-EOM-IP CCSD for core-ionized states and CVS-EOM-EE-CCSD for core-excited states;[41−44] the final decay states are described by EOM-DIP-CCSD (for nonresonant Auger) and EOM-IP-CCSD (for resonant Auger). Core electrons are frozen in the reference CCSD calculations.

Within the Feshbach−Fano treatment of metastable core-hole states,[36] two-body Dyson orbitals enter the expression for computing the decay widths ($\tilde{\Gamma}_\mu$) of these states. In this treatment, CVS is used to define a projector operator that separates the core-hole states from the continuum, making them bound with respect to electron loss. The decay channel is a product of a doubly (for nonresonant decay) or singly (for resonant decay) ionized molecular state times a free-electron state, described explicitly by a continuum function. The energy of Auger electrons is given by the energy difference between the core-hole state and target valence (doubly or singly) ionized state and the intensity of each decay channel is proportional to the corresponding $\tilde{\Gamma}_\mu$ (the width is inversely proportional to the decay rate because faster decay channels outcompete slower decay channels). The width of the core-hole state is given by the matrix element of the Hamiltonian between the initial and final state, which reduces to

$$\tilde{\Gamma}_\mu = 2\pi g_\alpha \int d\Omega_{\mathbf{k}} \left(\sum_p h_{p\mathbf{k}}{}^\mu \gamma^p + \frac{1}{2}\sum_{pqr} \langle pq||\mathbf{k}r\rangle^\mu \Gamma^{pq}_r \right) \left(\sum_p h_{p\mathbf{k}}{}^\mu \gamma^p + \frac{1}{2}\sum_{pqr} \langle \mathbf{k}r||pq\rangle^\mu \Gamma^r{}_{pq} \right) \tag{10}$$

where g_α is an electronic degeneracy factor, index μ marks the decay channel (i.e., a particular final state), γ and Γ are respective one- and two-body Dyson orbitals (Dyson geminals), and $h_{\mathbf{k}r}$ and $\langle \mathbf{k}r||pq\rangle$ are one- and two-electron integrals with index $\mathbf{k}$ denoting the free-electron state (represented by a continuum function) and indices p, q, r denoting bound molecular orbitals (represented by Gaussians). In this study, we represent the ejected electron state by the plane wave,[45] but the formalism can be generalized to more sophisticated treatments.

Recently, this treatment was combined with the EOM-CCSD theory and applied to calculations of resonant and nonresonant Auger spectra[36,45,46] as well as ICD.[47] The theoretical background of this treatment and details of the implementation can be found in ref 36.

Here we use the two-particle Dyson orbitals (Dyson geminals), eqs 8 and 9, to define natural Auger orbitals (NAOs) that provide the most compact orbital picture of the Auger decay. Following the same strategy as in the derivation of NTOs, we use SVD to reduce the three-index tensor Γ to a small number of three-orbital sets. For Γ^{pq}_r defined by eq 9, index r corresponds to the core hole and indices p and q to the valence holes in the target state (see Figure 2a). Hence, we first perform SVD on Γ^{pq}_r reshaped as the $M \times M^2$ matrix, $\Gamma_{r,pq}$, where pq represents a combined index $p \times M + q$ and M is the number of molecular orbitals (specifically, we use the $\beta\alpha\beta$ block; more on spin-symmetry below). As per eqs 3 and 5, this step yields the core NAO with its respective singular value. In a nonresonant Auger process, where the initial state has a single core vacancy, only one nonzero singular value is expected; however, in a resonant Auger decay, several core orbitals may be involved.

The core NAOs are given by the columns of matrix U, as per eq 5, and the corresponding columns of matrix V contain the information about the decay NAOs, p and q. To compute them, we reshape the corresponding column of V into the $M \times M$ matrix and perform SVD on it. This step yields pairs of orbitals that describe the target decay states. As we show below, this step often yields several nonzero singular values, reflecting multiconfigurational character of the target states. These NAOs represent a natural way to visualize the Auger decay and related processes (such as ICD and ETMD). Because Γ^{pq}_r enters the expression for decay widths, eq 10, the shapes of NAO can help to rationalize the trends in $\tilde{\Gamma}_\mu$. For example, when Γ^{pq}_r is represented by a single set of three NAOs, one can evaluate their contribution to the decay width as follows:

$$\tilde{\Gamma}_\mu \approx \frac{\pi}{2} g_\alpha (\sigma^1 \sigma^2 \langle \psi^{\mathrm{p}} \tilde{\psi}^{\mathrm{p}} || \psi^{\mathrm{h}} \mathbf{k}\rangle)^2 \tag{11}$$

where σ^1 and σ^2 are the leading singular values from the first and the second SVD steps, respectively, ψ^{h} is the core-hole NAO from the first step, and ψ^{p} and $\tilde{\psi}^{\mathrm{p}}$ are the two particle NAOs from the second SVD step. Note that symmetry selection rules apply to Auger processes—the product of the irrep of the initial hole state, the decay state, and the free-electron state should contain a fully symmetric irrep for the channel to be allowed; hence, symmetries of the initial and final states—or NAOs—determine the angular distributions of the Auger electrons.

As mentioned above, we use the $\Gamma^{p_\alpha q_\beta}_{r_\beta}$ block of Γ. In regular (i.e., nonresonant) Auger calculations, the ionized core-hole is of β spin by default, so that $\Gamma^{pq}_{r_\alpha}$ blocks are zero. For the target DIP states with M_S=0 (the default in Q-Chem), $\Gamma^{p_\alpha q_\beta}_{r_\beta} = \pm\Gamma^{p_\beta q_\alpha}_{r_\beta}$ for the triplet and singlet channels, respectively. Hence, for a closed-shell reference, using the $\Gamma^{p_\alpha q_\beta}_{r_\beta}$ block is equivalent to spin averaging. The second SVD procedure yields pairs of decay NAOs corresponding to $\alpha\beta$ configurations (the σ values for $\alpha\beta$ and $\beta\alpha$ decay states are identical).

To better understand the relationship between NAOs and the wave function amplitudes, we point out that the leading block of Γ^{pq}_r in a regular Auger decay is[36]

$$\Gamma^{ij}_K \approx l_K r_{ij} \tag{12}$$

where l and r are left CVS-IP and right EOM-DIP amplitudes, respectively, K denotes core orbitals, and i, j denote valence orbitals. Thus, the decay NAOs roughly follow the leading DIP amplitudes.

In a resonant Auger process, assuming that the ejected electron has α-spin, $\Gamma^{p_\beta q_\alpha}_{r_\beta} = \Gamma^{p_\alpha q_\beta}_{r_\beta} = \pm(\Gamma^{p_\alpha q_\beta}_{r_\alpha} = \Gamma^{p_\beta q_\alpha}_{r_\alpha})$. Thus, the core-hole orbital for the first step has identical α and β components, but only the β component is computed. The leading blocks of Γ^{pq}_r in resonant Auger decay are[36]

https://doi.org/10.1021/acs.jpclett.3c01966
J. Phys. Chem. Lett. 2023, 14, 8612−8619

Table 1. Water:[a] Ionization Energies of the Doubly Ionized States (eV), Energies of the Auger Electrons (eV), Partial Decay Widths (meV), Values of the Leading DIP Amplitudes, and PR_{NTO} Values from the First and Second SVD Steps

State	E^{DIP}	E_{Auger}[b]	$\tilde{\Gamma}$	Composition	PR_{NTO1}	PR_{NTO2}
$^1A_1$	41.58	498.56	17.72	$1b_2^{-2}$ (0.91), $3a_1^{-2}$ (0.19)	1	1.10
$^3A_2$	44.67	495.48	0.005	$1b_2^{-1}1b_1^{-1}$ (0.66)	1	2.00
$^1B_1$	48.76	491.39	13.46	$3a_1^{-1}1b_1^{-1}$ (0.67)	1	2.00

[a]MP2/aug-cc-pVTZ optimized structure; fully uncontracted 6-311(2+,+)G** basis set[52] was used for DIP and CVS EOM-IP. [b]Energies of Auger electrons computed using core IE of 540.15 eV.

$$\Gamma_J^{ai} \approx -l_J^a r_i \tag{13}$$

$$\Gamma_K^{ij} \approx -\sum_a l_K^a r_{ij}^a \tag{14}$$

where l and r are the left CVS-EE and right EOM-IP amplitudes, respectively. Eqs 13 and 14 provide dominant contributions for the participator and spectator decay, respectively.

The renormalized σ^2 represents the weights of a particular configuration in the total wave function. A useful quantity is participation ratio (PR_{NTO}), which quantifies how many orbitals (or orbital pairs) contribute to the wave function:[25,48]

$$PR_{NTO} = \frac{\left(\sum_K \sigma_K^2\right)^2}{\sum_K \sigma_K^4} \tag{15}$$

For example, PR_{NTO} = 1 when there is only one dominant amplitude for the core-hole state, PR_{NTO} = 2 for the two core-hole states, and so on.

We implemented this procedure in the Q-Chem electronic structure package[49,50] for nonresonant and resonant Auger decay. Additional details are given in the SI. We illustrate the utility of NAOs by application to water and benzene molecules, a model solvated hydroxide cluster, and a Mg-$(H_2O)_6^{2+}$ cluster. All calculations were done using the Q-Chem electronic structure package.[49] Q-Chem's symmetry notations are used.[51]

Table 1 shows the three lowest decay channels for core-ionized water, including their character based on the leading EOM-DIP-CCSD amplitudes (right vectors). The corresponding NAOs are shown in Figure 3; their PR_{NTO} values are reported in Table 1 . As one can see, the singular values for the first step (that yields the initial core-hole state) are very close to one, giving rise to PR_{NTO1} = 1. The shapes of the decay NAOs (orbitals from the second step) are similar to those of the canonical MOs, and their singular values and respective PR_{NTO}s are consistent with the leading amplitudes of the DIP states, as per eq 12 (Table 1). For example, the PR_{NTO} values for $^3A_2$ and $^1B_1$ are close to two, consistent with the $\alpha\beta$ and $\beta\alpha$ configurations of the DIP amplitudes. The DIP states derived from removing both electrons from the same orbital give rise to one decay pair whereas the DIP states derived by removing two electrons from different MOs give rise to two pairs of NAOs.

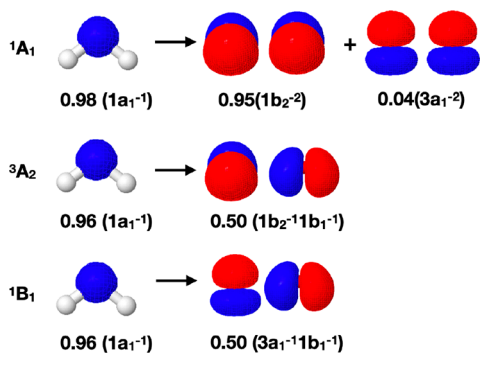

Figure 3. Natural Auger orbitals for the $^1A_1$, $^3A_2$, and $^1B_1$, decay channels of the $1s_O$-ionized state of water. Squared singular values from the first (left) and second (right) SVD steps are shown under the NAOs, along with the dominant electronic configurations (only $\alpha\beta$ decay NAOs are shown).

In contrast to water, benzene has six core orbitals, and each can contribute to Auger decay. This, along with high symmetry of benzene, gives rise to a rich Auger spectrum,[53−55] which we recently described and analyzed theoretically.[46] In the discussion below, we use the irreducible representations of the D_{2h} point group, the largest Abelian subgroup of the D_{6h} point group of benzene, following the convention in Q-Chem (the mapping to the D_{6h} symmetry labels is given in Figure S1 in the SI). Here we focus on NAO analysis of selected decay channels. Table 2 shows the energies of several doubly ionized states of benzene and their leading DIP amplitudes. Based on DIP amplitudes, the decay channels can be divided into three types: decay states corresponding to the ionization of doubly degenerate HOMO, decay states corresponding to ionization from HOMO and HOMO-1/HOMO-2, and decay states corresponding to the ionization from HOMO and HOMO-3.

Figure 4 shows the NAOs for the decay channels summarized in Table 2. For this example, the shapes of NAOs appear to be similar to those of canonical MOs. For decay channel (A), the first SVD yields a single singular value corresponding to the core-ionized $2a_g$ orbital. The second SVD shows that the main decay channel is derived by the removal of electrons from the $1b_{2g}$ and $1b_{3g}$ HOMOs of benzene, consistent with the amplitudes of the $^1B_{1g}$ DIP state. Likewise, we see that channel (B) corresponds to the core hole of B_{3u} symmetry and two decay channels with doubly ionized $1b_{2g}$ or $1b_{3g}$ HOMOs. The analysis shows that channels (C)−(E) correspond to ionization from the HOMO and lower orbitals. For this example, the NAO analysis closely follows the DIP amplitudes of the decay channels, and the shapes of NAOs are similar to those of the canonical Hartree−Fock MOs or the natural orbitals of the DIP states;[46] however, the examples below illustrate that this is not always the case.

As the next example, we consider the resonant Auger decay in benzene. The brightest peak in the XAS of benzene corresponds to the $1s_c \rightarrow \pi^*$ transition of B_{1u} symmetry (traditionally called A peak).[56,57] In our calculations, this state appears at 286.9 eV. Consistent with the orbital degeneracy patterns, NTO analysis for this transition[56,57] yields several pairs of NTOs (PR_{NTO} = 2.45). Figure 5 shows NAOs for the Auger decay of this state. Consistent with XAS NTOs (see Figure S2 in the SI), we obtain two core holes with equal

https://doi.org/10.1021/acs.jpclett.3c01966
J. Phys. Chem. Lett. 2023, 14, 8612−8619

Table 2. Benzene:[a] Ionization Energies of the Doubly Ionized States (eV) and Core-Ionized States (eV), the Corresponding Energies of the Auger Electrons (eV), Partial Decay Widths (meV), the Values of the Leading DIP Amplitudes, and PR_{NTO} Values from the First and Second SVD Steps

State	E^{DIP}	core	E	E_{Auger}	$\tilde{\Gamma}$	Composition	PR_{NTO1}	PR_{NTO2}
$^1B_{1g}$	25.40	$2a_g^{-1}$	291.20	265.80	0.130	$1b_{2g}^{-1}1b_{3g}^{-1}(0.66)$	1.11	2.01
^1A_g	25.40	$2b_{3u}^{-1}$	291.18	265.78	0.760	$1b_{2g}^{-2}(0.66)$, $1b_{3g}^{-2}(0.66)$	1.12	2.01
$^3B_{3g}$	27.75	$1b_{2u}^{-1}$	291.24	263.50	0.003	$3b_{1g}^{-1}1b_{2g}^{-1}$ (0.47), $6a_g^{-1}1b_{3g}^{-1}$ (0.47)	1.07	4.14
$^3B_{3u}$	27.80	$1b_{1g}^{-1}$	291.20	263.40	0.001	$1b_{2g}^{-1}1b_{1u}^{-1}$ (0.67)	1.05	2.00
^1A_u	29.80	$1a_g^{-1}$	291.26	261.47	0.040	$4b_{2u}^{-1}1b_{2g}^{-1}$ (0.47), $5b_{3u}^{-1}1b_{3g}^{-1}$ (0.47)	1.08	4.00

[a]RI-MP2/cc-pVTZ optimized structure; 6-311G** basis set was used for DIP and CVS EOM-IP.

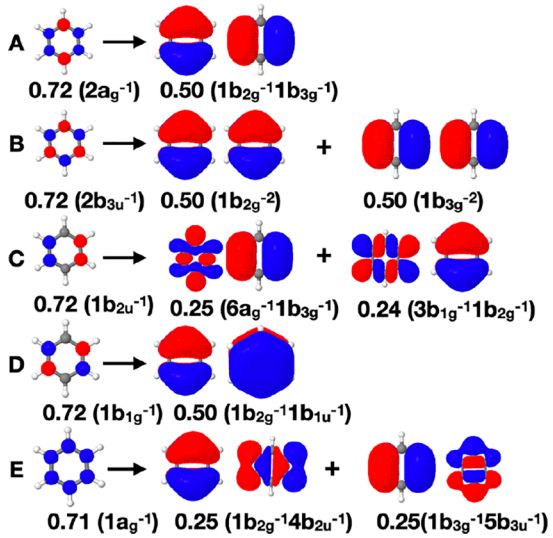

Figure 4. Natural Auger orbitals for selected decay channels in $1s_C$-ionized benzene. Squared singular values from the first (left) and second (right) SVD steps are shown along with the dominant electronic configurations (only $\alpha\beta$ decay NAOs are shown).

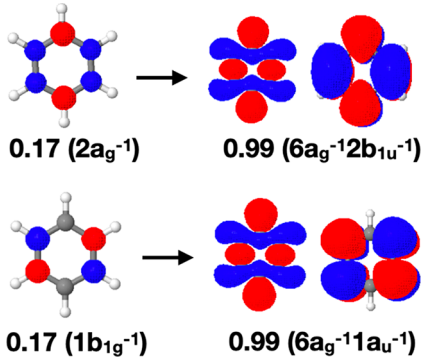

Figure 5. Natural Auger orbitals for resonant Auger decay in benzene. The initial state is the B_{1u} core-excited state with excitation energy 286.9 eV (peak A in XAS). Squared singular values from the first (left) and second (right) SVD steps are shown along with the dominant electronic configurations (only $\beta \rightarrow \alpha\beta$ NAOs are shown). The PR_{NTO} values from the first SVD is 2.51, consistent with the CVS EOM-EE amplitudes, and that from the second SVD is 1.02, each corresponding to the single valence hole for every dominant core hole.

weights and two decay NAOs, one of which is the π^* LUMO and the second is a lower valence orbital (HOMO-1). The large σ^2 value for the second step reflects that the EOM-IP decay state is dominated by a single valence hole. According to this picture, this decay channel corresponds to the participator decay. We note that in the resonant Auger decay, one can consider an alternative definition of NAOs, i.e., by first performing SVD for $\Gamma_{rp,q}$. Such a procedure yields NAOs that look like a union of NTOs for the XAS transition and a valence hole, as per eq 13; this is illustrated in Figure S3 in the SI.

Finally, Figure S4 in the SI shows NAOs for the spectator decay in benzene. We note that in this case, the singular values are much smaller compared to the participator decay.

Our next example is a model cluster of hydroxide solvated with five water molecules (the structure is taken from an ab initio molecular dynamics equilibrium trajectory[58]). We consider Auger decay of the core-ionized $1s_O$ state of hydroxide—this state has the lowest IE (534.02 eV) of the six $1s_O$ states of the cluster. Table 3 shows three lowest-energy

Table 3. $OH^-(H_2O)_5$ Cluster:[a] Ionization Energies of the Singlet Doubly Ionized States (eV), Energies of the Auger Electrons (eV), Partial Decay Widths (meV), and PR_{NTO} Values from the First and Second SVD Steps

State	E^{DIP}	E_{Auger}	$\tilde{\Gamma}$	PR_{NTO1}	PR_{NTO2}
1^1A	16.66	517.36	0.007	1	2.04
2^1A	16.79	517.23	0.005	1	2.10
3^1A	16.93	517.10	0.002	1	2.03

[a]6-311G basis set was used for DIP and CVS EOM-IP; core IE is 534.02 eV.

singlet decay channels (corresponding to the fastest Auger electrons). In this case, the decay states can be either localized on hydroxide or on the nearby waters or both. The DIP amplitudes (see Figure S7 in the SI) involve many transitions, making the characterization of the decay channels difficult. In contrast, the NAO analysis yields a much more compact picture. Figure 6 shows NAOs for the three lowest singlet decay channels of the cluster. The analysis of the triplet decay channels is given in the SI. As one can see, all three channels have contributions both from the hydroxide orbitals and from the waters. The relative weight of the hydroxide is the largest in the first channel and the smallest in the third channel, which correlates with the computed decay widths that decrease in this sequence 1 > 2 > 3. Based on the shapes of the NAOs, these three channels appear to be of mixed Auger and ICD character.

Finally, we also analyzed the decay of the inner-valence vacancy in a model $Mg(H_2O)_6^{2+}$ cluster (using a slightly distorted octahedral structure). The initial state is a 2*s* vacancy in Mg. Without solvating waters, this state is electronically stable, but it can decay via ICD in solution producing ionized water molecules. Table 4 lists the relevant data, and Figure 7 shows the NAOs for the three lowest decay channels. As one can see, the NAOs show that the decay is dominated by the water molecules.

https://doi.org/10.1021/acs.jpclett.3c01966
J. Phys. Chem. Lett. 2023, 14, 8612−8619

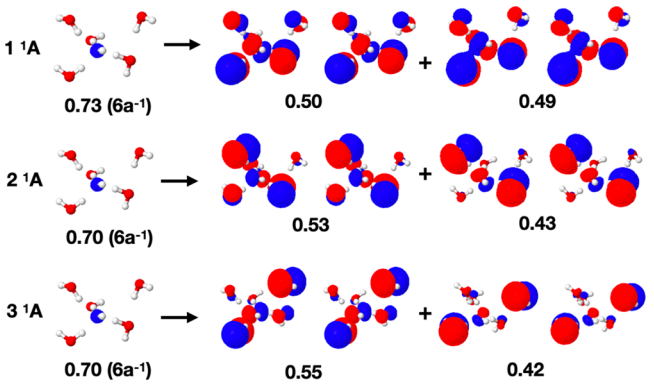

Figure 6. Natural Auger orbitals for the first three singlet decay channels of the $1s_O$-ionized state of $OH^-(aq)$. Singular values from the first (left) and second (right) SVD steps are shown under the NAOs, along with the dominant electronic configurations.

Table 4. $Mg(H_2O)_6^{2+}$ Cluster:[a] Ionization Energies of the Singlet Doubly Ionized States (eV), Energies of the Auger Electrons (eV), Partial Decay Widths (10^{-5} meV), and PR_{NTO} Values from the First and Second SVD Steps

State	E^{DIP}	E_{Auger}	$\tilde{\Gamma}$	PR_{NTO1}	PR_{NTO2}
1^1A	46.24	59.26	5.62	1	2.07
2^1A	46.24	59.26	4.54	1	4.02
3^1A	46.24	59.26	3.57	1	3.99

[a]Geometry optimized with RI-MP2/cc-pVTZ; 6-311G** basis set was used for DIP and CVS EOM-IP; IE of Mg(2*s*) is 105.51 eV.

In conclusion, we presented an extension of the molecular orbital framework for two-electron processes such as Auger–Meitner decay and ICD. The theory is based on two-body Dyson orbitals (Dyson geminals) connecting the initial (core-ionized or core-excited) and final decay states (doubly or singly ionized). Two sequential singular-value decompositions of the two-body Dyson orbitals yield a small number of three-orbital sets, which provide a compact representation of the decay process. This new tool enables casting two-electron decay involving correlated many-body wave functions into a simple yet rigorous molecular orbital picture, thus facilitating analysis and providing insight into X-ray induced processes. Further work will involve developing the relationships between the NAOs and physical observables such as, for example, angular distributions of Auger electrons.

■ ASSOCIATED CONTENT

Supporting Information

The Supporting Information is available free of charge at https://pubs.acs.org/doi/10.1021/acs.jpclett.3c01966.

Description of the algorithms; relevant Cartesian coordinates; and additional results for decay channels in studied systems (PDF)

■ AUTHOR INFORMATION

Corresponding Author

Anna I. Krylov − *Department of Chemistry, University of Southern California, Los Angeles, California 90089, United States;* orcid.org/0000-0001-6788-5016; Email: krylov@usc.edu

Authors

Nayanthara K. Jayadev − *Department of Chemistry, University of Southern California, Los Angeles, California 90089, United States;* orcid.org/0000-0003-1174-5668

Wojciech Skomorowski − *Centre of New Technologies, University of Warsaw, 02-097 Warsaw, Poland;* orcid.org/0000-0002-0364-435X

Complete contact information is available at: https://pubs.acs.org/10.1021/acs.jpclett.3c01966

Notes

The authors declare the following competing financial interest(s): A.I.K. is the president and a part-owner of Q-Chem, Inc.

■ ACKNOWLEDGMENTS

We thank Dr. Pavel Pokhilko for his help with validating our implementation. This work was supported in Los Angeles by the U.S. National Science Foundation (No. CHE-2154482 to A.I.K.)

■ REFERENCES

(1) Krylov, A. I. From orbitals to observables and back. *J. Chem. Phys.* **2020**, *153*, 080901.

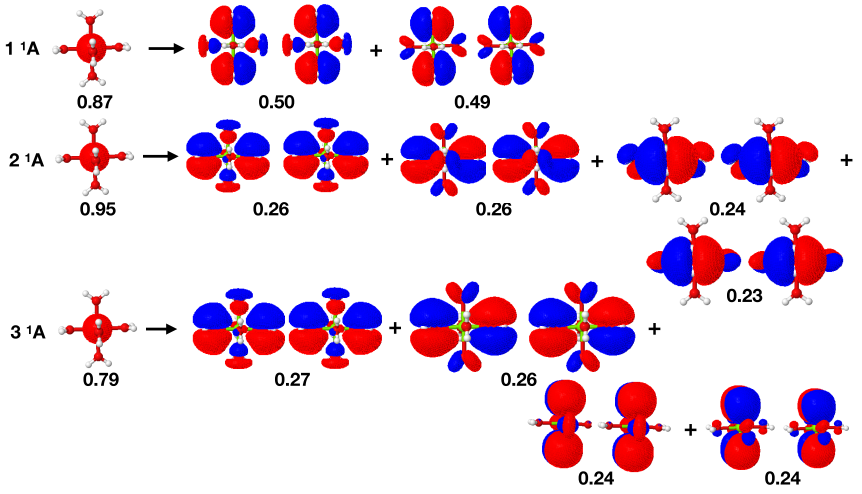

Figure 7. Natural Auger orbitals for the three lowest ICD channels of a 2*s* vacancy in a model $Mg(H_2O)_6^{2+}$ cluster.

https://doi.org/10.1021/acs.jpclett.3c01966
J. Phys. Chem. Lett. 2023, 14, 8612−8619

(2) Santra, R. Imaging molecular orbitals using photoionization. *Chem. Phys.* **2006**, *329*, 357−364.
(3) Puschnig, P.; Berkebile, S.; Fleming, A. J.; Koller, G.; Emtsev, K.; Seyller, T.; Riley, J. D.; Ambrosch-Draxl, C.; Netzer, F. P.; Ramsey, M. G. Reconstruction of molecular orbital densities from photoemission data. *Science* **2009**, *326*, 702−706.
(4) Weiß, S.; Lüftner, D.; Ules, T.; Reinisch, E. M.; Kaser, H.; Gottwald, A.; Richter, M.; Soubatch, S.; Koller, G.; Ramsey, M. G.; et al. Exploring three-dimensional orbital imaging with energy-dependent photoemission tomography. *Nat. Comm* **2015**, *6*, 8287.
(5) Goscinski, O.; Lindner, P. Natural spin-orbitals and generalized overlap amplitudes. *J. Math. Phys.* **1970**, *11*, 1313−1317.
(6) Linderberg, J.; Öhrn, Y. *Propagators in quantum chemistry*; Academic: London, 1973.
(7) Oana, C. M.; Krylov, A. I. Dyson orbitals for ionization from the ground and electronically excited states within equation-of-motion coupled-cluster formalism: Theory, implementation, and examples. *J. Chem. Phys.* **2007**, *127*, 234106.
(8) Gozem, S.; Gunina, A. O.; Ichino, T.; Osborn, D. L.; Stanton, J. F.; Krylov, A. I. Photoelectron wave function in photoionization: Plane wave or Coulomb wave? *J. Phys. Chem. Lett.* **2015**, *6*, 4532−4540.
(9) Jagau, T.-C.; Krylov, A. I. Characterizing metastable states beyond energies and lifetimes: Dyson orbitals and transition dipole moments. *J. Chem. Phys.* **2016**, *144*, 054113.
(10) Ortiz, J. V. Dyson-orbital concepts for description of electrons in molecules. *J. Chem. Phys.* **2020**, *153*, 070902.
(11) Luzanov, A. V.; Sukhorukov, A. A.; Umanskii, V. E. Application of transition density matrix for analysis of excited states. *Theor. Exp. Chem.* **1976**, *10*, 354−361.
(12) Luzanov, A. V.; Pedash, V. F. Interpretation of excited states using charge-transfer number. *Theor. Exp. Chem.* **1980**, *15*, 338−341.
(13) Pokhilko, P.; Krylov, A. I. Quantitative El-Sayed rules for many-body wavefunctions from spinless transition density matrices. *J. Phys. Chem. Lett.* **2019**, *10*, 4857−4862.
(14) Nanda, K. D.; Krylov, A. I. Visualizing the contributions of virtual states to two-photon absorption cross-sections by natural transition orbitals of response transition density matrices. *J. Phys. Chem. Lett.* **2017**, *8*, 3256−3265.
(15) Nanda, K. D.; Krylov, A. I. A simple molecular orbital picture of RIXS distilled from many-body damped response theory. *J. Chem. Phys.* **2020**, *152*, 244118.
(16) Nanda, K. D.; Krylov, A. I. The orbital picture of the first dipole hyperpolarizability from many-body response theory. *J. Chem. Phys.* **2021**, *154*, 184109.
(17) de Wergifosse, M.; Grimme, S. A unified strategy for the chemically intuitive interpretation of molecular optical response properties. *J. Chem. Theory Comput.* **2020**, *16*, 7709−7720.
(18) McWeeny, R. *Methods of Molecular Quantum Mechanics*, 2nd ed.; Academic Press: 1992.
(19) Mestechkin, M. M. *Metod matritsy plotnosti v teorii molekul*; Naukova Dumka: Kyiv, 1977.
(20) Helgaker, T.; Jørgensen, P.; Olsen, J. *Molecular electronic structure theory*; Wiley & Sons: 2000.
(21) Gozem, S.; Krylov, A. I. The ezSpectra suite: An easy-to-use toolkit for spectroscopy modeling WIREs: *Comput. Mol. Sci.* **2022**, *12*, No. e1546.
(22) Bäppler, S. A.; Plasser, F.; Wormit, M.; Dreuw, A. Exciton analysis of many-body wave functions: Bridging the gap between the quasiparticle and molecular orbital pictures. *Phys. Rev. A* **2014**, *90*, 052521.
(23) Mewes, S. A.; Plasser, F.; Krylov, A.; Dreuw, A. Benchmarking excited-state calculations using exciton properties. *J. Chem. Theory Comput.* **2018**, *14*, 710−725.
(24) Kimber, P.; Plasser, F. Toward an understanding of electronic excitation energies beyond the molecular orbital picture. *Phys. Chem. Chem. Phys.* **2020**, *22*, 6058−6080.
(25) Plasser, F. Entanglement entropy of electronic excitations. *J. Chem. Phys.* **2016**, *144*, 194107.
(26) Skomorowski, W.; Krylov, A. I. Real and imaginary excitons: Making sense of resonance wavefunctions by using reduced state and transition density matrices. *J. Phys. Chem. Lett.* **2018**, *9*, 4101−4108.
(27) Meitner, L. About the β ray spectra and their connection with the γ radiation. *Z. Phys.* **1922**, *11*, 35−54.
(28) Auger, P. Secondary β-rays produced in a gas by X-rays Comptes Rendus. *Acad. Sci. Paris* **1923**, *177*, 169.
(29) Cederbaum, L. S.; Zobeley, J.; Tarantelli, F. Giant intermolecular decay and fragmentation of clusters. *Phys. Rev. Lett.* **1997**, *79*, 4778−4781.
(30) Jahnke, T.; Hergenhahn, U.; Winter, B.; Dörner, R.; Frühling, U.; Demekhin, P. V.; Gokhberg, K.; Cederbaum, L. S.; Ehresmann, A.; Knie, A.; et al. Interatomic and intermolecular Coulombic decay. *Chem. Rev.* **2020**, *120*, 11295−11369.
(31) Zobeley, J.; Santra, R.; Cederbaum, L. S. Electronic decay in weakly bound heteroclusters: Energy transfer versus electron transfer. *J. Chem. Phys.* **2001**, *115*, 5076−5088.
(32) Ku, A.; Facca, V. J.; Cai, Z.; Reilly, R. M. Auger electrons for cancer therapy—a review. *EJNMMI Radiopharm. Chem.* **2019**, *4*, 27.
(33) Pirovano, G.; Jannetti, S. A.; Carter, L. M.; Sadique, A.; Kossatz, S.; Guru, N.; Demétrio De Souza França, P.; Maeda, M.; Zeglis, B. M.; Lewis, J. S.; et al. Targeted brain tumor radiotherapy using an Auger emitter. *Clin. Cancer Res.* **2020**, *26*, 2871−2881.
(34) Borbinha, J.; Vaz, P.; Di Maria, S. Dosimetric assessment in different tumour phenotypes with Auger electron emitting radionuclides: ^{99m}Tc, ^{125}I, ^{161}Tb, and ^{177}Lu Radiat. *Phys. Chem.* **2020**, *172*, 108763.
(35) Pirovano, G.; Wilson, T. C.; Reiner, T. Auger: The future of precision medicine. *Nucl. Med. and Bio.* **2021**, *96*, 50−53.
(36) Skomorowski, W.; Krylov, A. I. Feshbach-Fano approach for calculation of Auger decay rates using equation-of-motion coupled-cluster wave functions. I. Theory and implementation. *J. Chem. Phys.* **2021**, *154*, 084124.
(37) Ågren, H. On the interpretation of molecular valence Auger spectra. *J. Chem. Phys.* **1981**, *75*, 1267−1283.
(38) Manne, R.; Ågren, H. Auger transition amplitudes from general many-electron wavefunctions. *Chem. Phys.* **1985**, *93*, 201−208.
(39) Ågren, H.; Cesar, A.; Liegener, C.-M. Theory of molecullar Auger spectra. *Adv. Quantum Chem.* **1992**, *23*, 1−82.
(40) Cederbaum, L. S.; Domcke, W.; Schirmer, J. Many-body theory of core holes. *Phys. Rev. A* **1980**, *22*, 206.
(41) Coriani, S.; Koch, H. Communication: X-ray absorption spectra and core-ionization potentials within a core-valence separated coupled cluster framework. *J. Chem. Phys.* **2015**, *143*, 181103.
(42) Coriani, S.; Koch, H. Erratum: "Communication: X-ray absorption spectra and core-ionization potentials within a core-valence separated coupled cluster framework. *J. Chem. Phys.* **2016**, *145*, 149901.
(43) Vidal, M. L.; Feng, X.; Epifanovsky, E.; Krylov, A. I.; Coriani, S. A new and efficient equation-of-motion coupled-cluster framework for core-excited and core-ionized states. *J. Chem. Theory Comput.* **2019**, *15*, 3117−3133.
(44) Vidal, M. L.; Krylov, A. I.; Coriani, S. Dyson orbitals within the fc-CVS-EOM-CCSD framework: theory and application to X-ray photoelectron spectroscopy of ground and excited states. *Phys. Chem. Chem. Phys.* **2020**, *22*, 2693−2703.
(45) Skomorowski, W.; Krylov, A. I. Feshbach-Fano approach for calculation of Auger decay rates using equation-of-motion coupled-cluster wave functions. II. Numerical examples and benchmarks. *J. Chem. Phys.* **2021**, *154*, 084125.
(46) Jayadev, N. K.; Ferino-Pérez, A.; Matz, F.; Krylov, A. I.; Jagau, T.-C. The Auger spectrum of benzene. *J. Chem. Phys.* **2023**, *158*, 064109.
(47) Parravicini, V.; Jagau, T.-C. Interatomic and intermolecular Coulombic decay rates from equation-of-motion coupled-cluster theory with complex basis functions. *arXiv*, 2023. https://arxiv.org/abs/2305.10186.

https://doi.org/10.1021/acs.jpclett.3c01966
J. Phys. Chem. Lett. 2023, 14, 8612−8619

(48) Plasser, F.; Lischka, H. Analysis of excitonic and charge transfer interactions from quantum chemical calculations. *J. Chem. Theory Comput.* **2012**, *8*, 2777−2789.
(49) Epifanovsky, E.; Gilbert, A. T. B.; Feng, X.; Lee, J.; Mao, Y.; Mardirossian, N.; Pokhilko, P.; White, A. F.; Coons, M. P.; Dempwolff, A. L.; et al. Software for the frontiers of quantum chemistry: An overview of developments in the Q-Chem 5 package. *J. Chem. Phys.* **2021**, *155*, 084801.
(50) Krylov, A. I.; Gill, P. M. W. Q-Chem: An engine for innovation WIREs: *Comput. Mol. Sci.* **2013**, *3*, 317−326.
(51) Depending on molecular orientation, symmetry labels corresponding to the same orbital or vibrational mode may be different. Q-Chem's standard molecular orientation is different from that of Mulliken.[59] For example, Q-Chem would place the water molecule in the *xz* plane instead of the *yz*. Consequently, for C_{2v} symmetry, b_1 and b_2 labels are flipped. More details can be found at http://iopenshell.usc.edu/resources/howto/symmetry/. To avoid confusion with different molecular orientations and relabeling the states, here we report the structures and symmetry labels following the Q-Chem's notations.
(52) Sarangi, R.; Vidal, M. L.; Coriani, S.; Krylov, A. I. On the basis set selection for calculations of core-level states: Different strategies to balance cost and accuracy. *Mol. Phys.* **2020**, *118*, No. e1769872.
(53) Spohr, R.; Bergmark, T.; Magnusson, N.; Werme, L. O.; Nordling, C.; Siegbahn, K. Electron spectroscopic investigation of Auger processes in bromine substituted methanes and some hydrocarbons. *Phys. Scr.* **1970**, *2*, 31.
(54) Rennie, E. E.; Kempgens, B.; Köppe, H. M.; Hergenhahn, U.; Feldhaus, J.; Itchkawitz, B. S.; Kilcoyne, A. L. D.; Kivimäki, A.; Maier, K.; Piancastelli, M. N.; et al. A comprehensive photoabsorption, photoionization, and shake-up excitation study of the C1s cross section of benzene. *J. Chem. Phys.* **2000**, *113*, 7362−7375.
(55) Carniato, S.; Selles, P.; Ferté, A.; Berrah, N.; Wuosmaa, A. H.; Nakano, M.; Hikosaka, Y.; Ito, K.; Žitnik, M.; Bučar, K.; et al. Single photon simultaneous K-shell ionization/excitation in C_6H_6: Experiment and theory. *J. Phys. B* **2020**, *53*, 244010.
(56) Nanda, K. D.; Vidal, M. L.; Faber, R.; Coriani, S.; Krylov, A. I. How to stay out of trouble in RIXS calculations within the equation-of-motion coupled-cluster damped response theory? Safe hitchhiking in the excitation manifold by means of core-valence separation. *Phys. Chem. Chem. Phys.* **2020**, *22*, 2629−2641.
(57) Vidal, M. L.; Epshtein, M.; Scutelnic, V.; Yang, Z.; Xue, T.; Leone, S. R.; Krylov, A. I.; Coriani, S. The interplay of open-shell spin-coupling and Jahn-Teller distortion in benzene radical cation probed by x-ray spectroscopy. *J. Phys. Chem. A* **2020**, *124*, 9532−9541.
(58) Kjellsson, L.; Nanda, K. D.; Rubensson, J.-E.; Doumy, G.; Southworth, S. H.; Ho, P. J.; March, A. M.; Al Haddad, A.; Kumagai, Y.; Tu, M.-F.; et al. Resonant inelastic x-ray scattering reveals hidden local transitions of the aqueous OH radical. *Phys. Rev. Lett.* **2020**, *124*, 236001.
(59) Mulliken, R. S. Report on notation for the spectra of polyatomic molecules. *J. Chem. Phys.* **1955**, *23*, 1997−2011.

https://doi.org/10.1021/acs.jpclett.3c01966
J. Phys. Chem. Lett. 2023, 14, 8612−8619